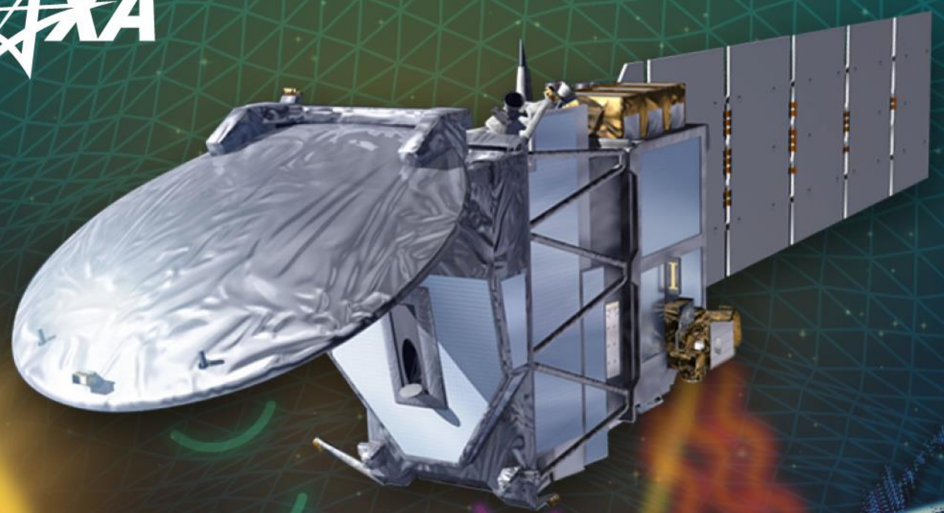

ESA-JAXA Pre-Launch EarthCARE Science and Validation Workshop

13 – 17 November 2023 | ESA-ESRIN, Frascati (Rome), Italy

Spaceborne lidars for Ocean Color studies: the results of the COLOR project from the perspective of the EarthCARE mission

D. Dionisi[1], S. Bucci[2], C. Cesarini[1], S. Colella[1], D. D'Alimonte[3], L. Di Ciolo[2], P. Di Girolamo[4], M. Di Paolantonio[1], N. Franco[4], G. Gostinicchi[2], T. Kajiyama[3], G. L. Liberti[1], E. Organelli[1], R. Santoleri[1]

1 - Consiglio Nazionale delle Ricerche, Istituto di Scienze Marine, Rome, Italy
2 - Serco Italia S.p.A., Frascati, Italy
3 - AEQUORA, Lisbon, Portugal
4 - Università degli Studi della Basilicata, Potenza, Italy

Introduction

❖ Scientific context

Demonstrated opportunity for future OC applications (IOCS, 2019)

Cloud Aerosol Lidar for Global Scale Observations of the Ocean-Land-Atmosphere System – CALIGOLA – ASI three-Year Activity Plan (2021-2023)

First investigations on **CALIOP subsurface bins** (Shi and Wang, 2008)

CALIOP Integrated **subsurface backscatter vs chlorophyll-a concentration** (Lu et al., 2014)

Going beyond standard ocean color observation: Lidar and Polarimetry (Jamet et al., 2019)

Assessment of the oceanic surface layer's optical properties through CALIOP (2020-2022)

earthcare

2008 2010 2012 2014 2016 2018 2020 2022 2024

Ocean particulate backscatter from Caliop

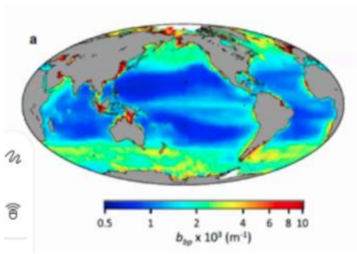

Behrenfeld et al., 2013

Annual cycle of polar phytoplankton **biomass**

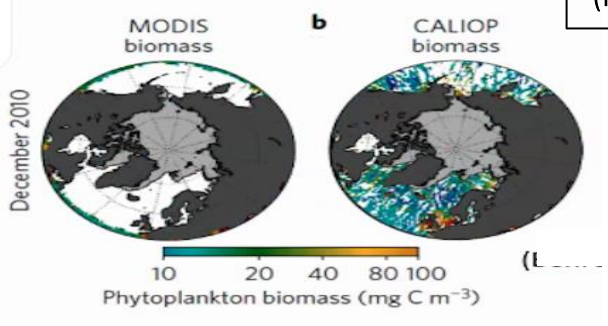

Behrenfeld et al., 2017

New ***lidar era*** in satellite oceanography (Hostetler et al., 2018)

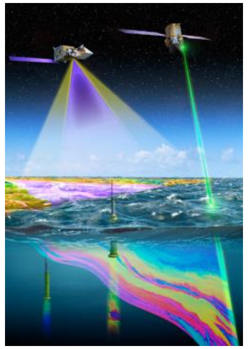

Ocean subsurface observations through ICEsat-2 (Lu et al., 2019)

CALIOP δ_T used as an oceanic variable for the ocean particulate optical properties (Dionisi et al., 2020)

GUANLAN mission for space oceanography (S. Wu, Aeolus cal/val meeting, 2020)

Vertical distribution of phytoplankton optical properties through **CALIOP** and **ICEsat-2** measurements (Lu et al., 2021)

AEOLUS OC prototype product (**COLOR** project)

Satellite lidars can complement passive ocean color data

Introduction

❖ Scientific context

The information content in the water leaving reflectances in the ~350 to 400 nm interval is **crucial** to distinguish *dissolved organic material* from chlorophyll in the upper ocean. The downward transport of organic material is a **key process in Earth's carbon cycle** and both affects, and is affected by, climate change. Chromophoric Dissolved Organic Matter (**CDOM**) is the most relevant contributor to the light absorption at 355 nm.

Lack of the UV information of past and current Ocean Color sensors

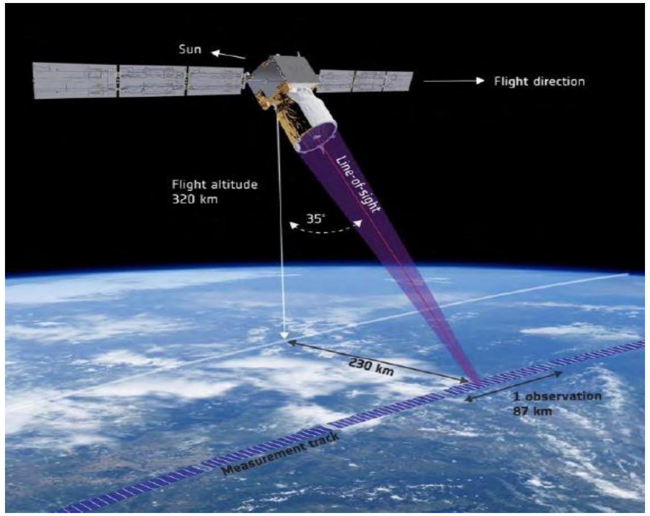

AEOLUS gives the opportunity to investigate the signal backscattered by the ocean sub-surface:

- ❑ First orbiting HSRL lidar
- ❑ Ocean subsurface information content in the UV
- ❑ The line-of-sight (LOS) points 35º from nadir

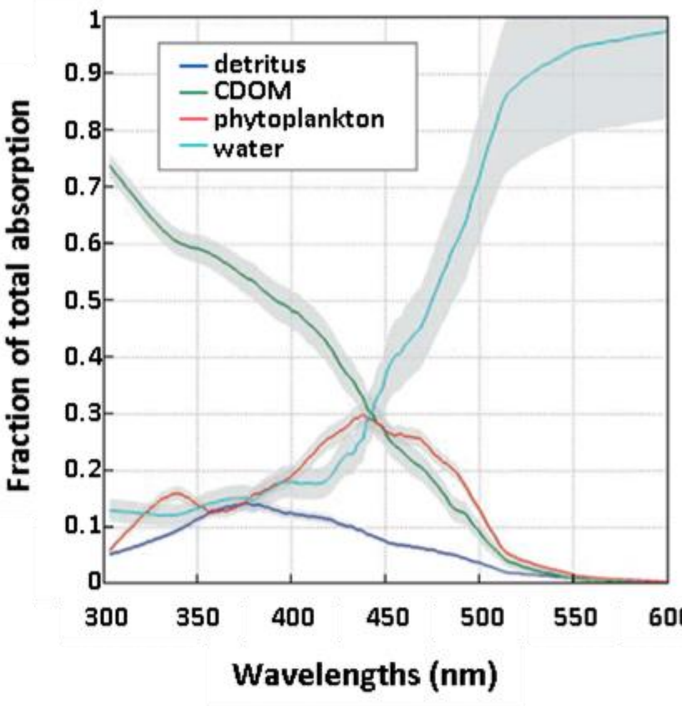

Outline

COLOR (***C****DOM-proxy retrieval from aeO****L****us Obse****R****vations)* was a feasibility study approved by **ESA** within the **Aeolus+ Innovation program** (ESA AO/1-9544/20/I/NS). **March 2021 - April 2023.** (ESA project responsible M.H.Rio)

Objective: COLOR proposes to evaluate and document the **feasibility** of deriving an **in-water AEOLUS product** at 355 nm

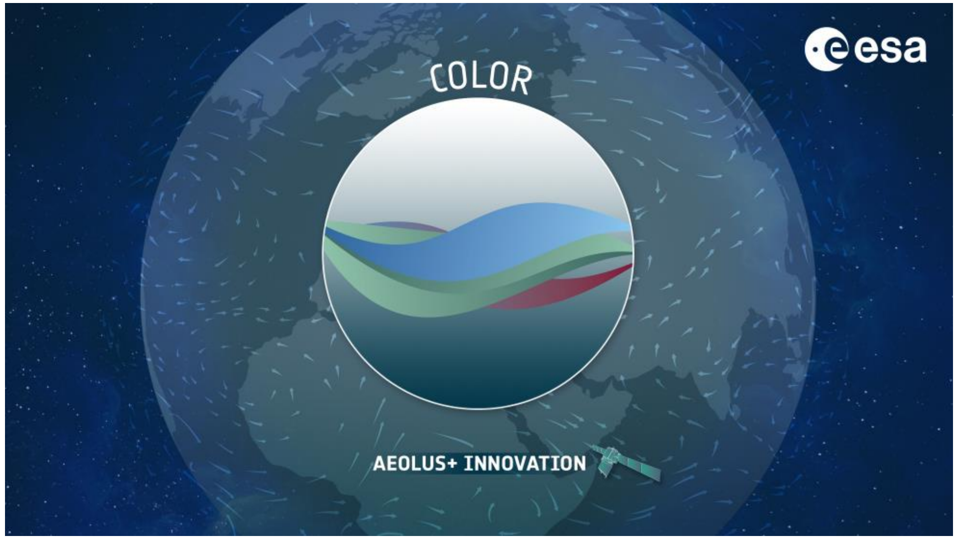

Consortium

- Institute of Marine Sciences (ISMAR) - CNR
- University of Basilicata
- Aequora
- Serco Italia SpA

Methods

❖ COLOR general approach

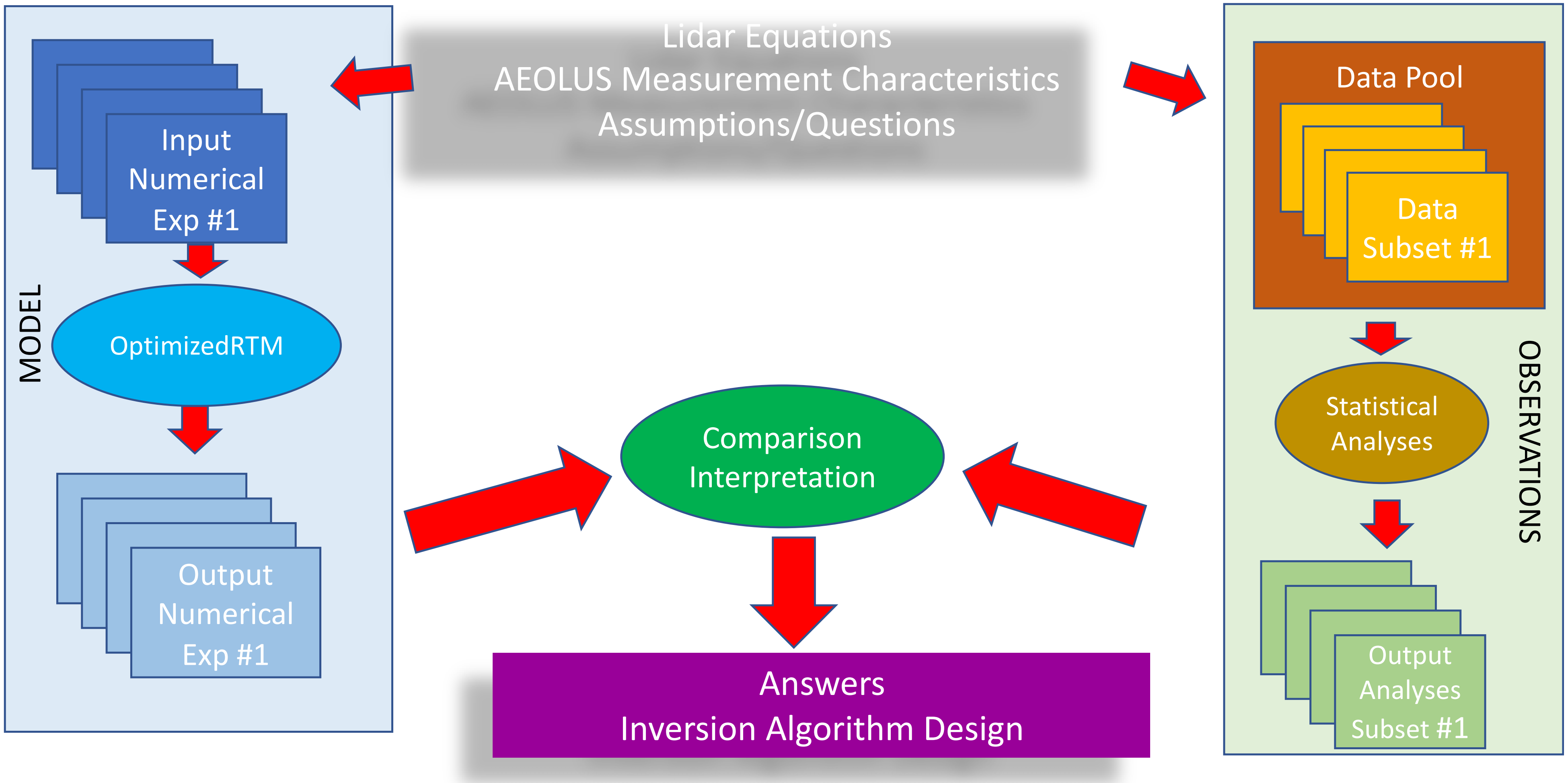

Methods

❖ LiOC in-water forward model

Lidar simulation code for Ocean Color applications (**LiOC**) developed fully accounting for ALADIN characteristics

LiOC components: $P_n = P_n^s + P_n^b + P_n^w$

- <u>At the **surface**:</u> negligible contribution of the reflected signal for wind speed up to the formation of white caps (~8 ms^{-1})
- <u>At the **bottom**:</u> negligible contribution of bottom effects in oligotrophic conditions for depth ≤ 80 m.
- <u>In the **water columns**:</u> MC ray tracing is driven by seawater Inherent Optical Properties.

$$b_{tot} = b_w + b_p(\text{Chl–a})$$
$$a_{tot} = a_w + \boldsymbol{\Delta a}$$
$$c_{tot} = a_{tot} + b_{tot}$$
$$\tilde{\beta}_p(\Psi, \text{Chl–a})$$

→ LiOC → $\mathbf{P_n}$

D'Alimonte et al., 2023 (submitted to Optic Express)

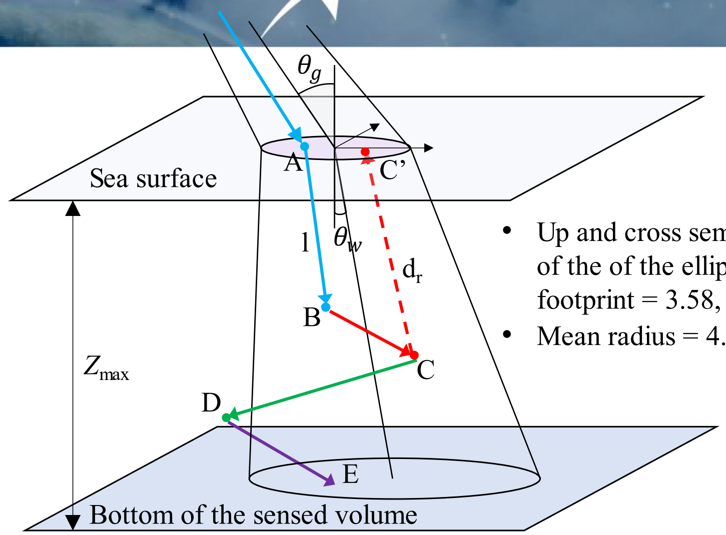

- Up and cross semi-axis of the of the ellipse footprint = 3.58, 4.49 [m]
- Mean radius = 4.03 [m]

Ray-tracing scheme

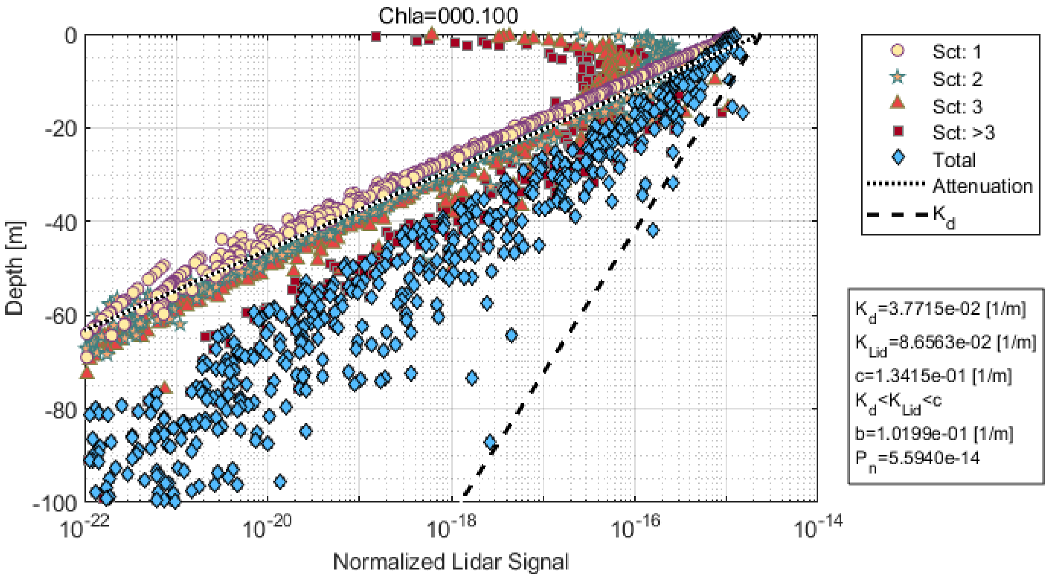

Methods

❖ AEOLUS in-water algorithm

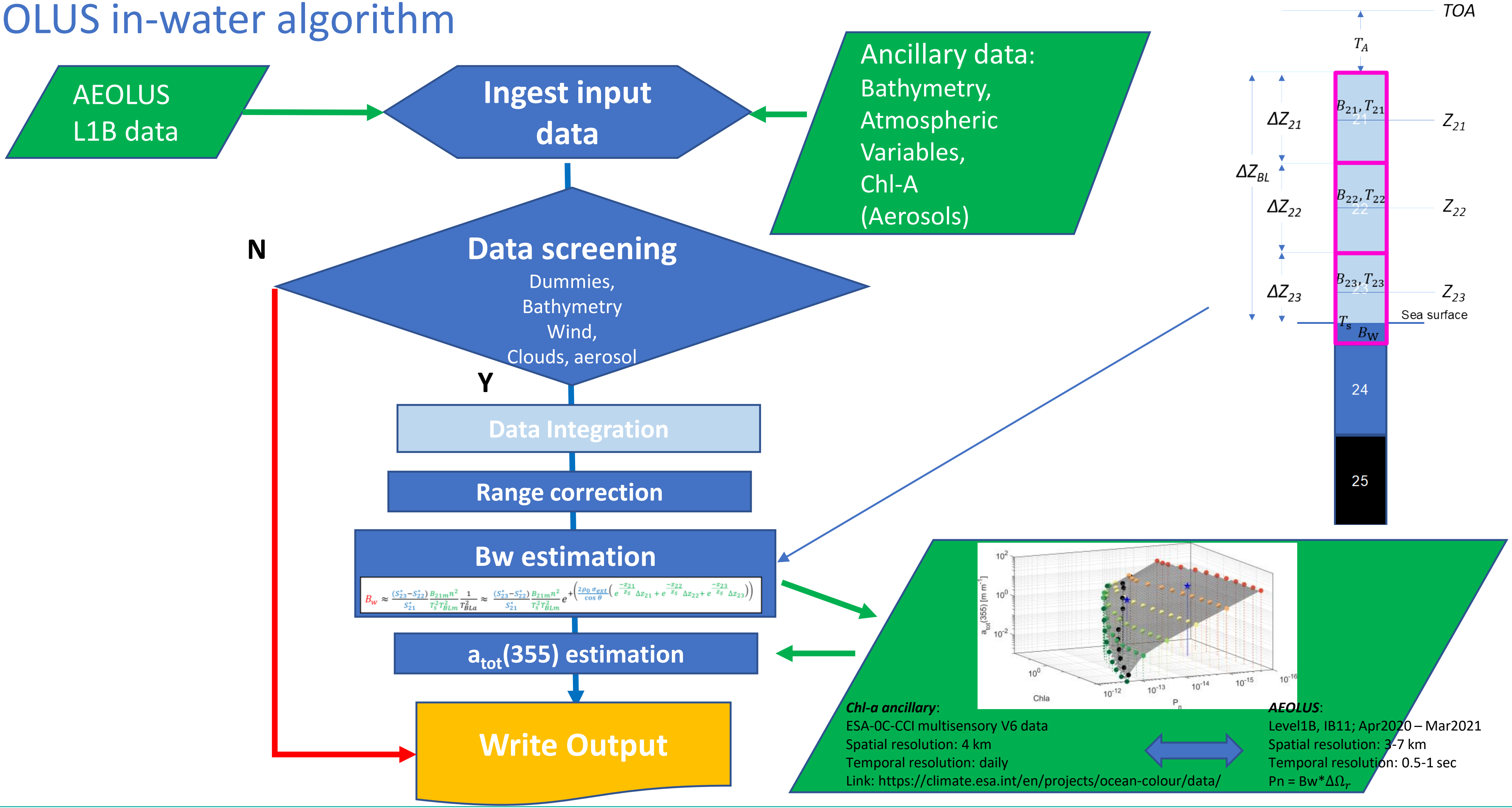

Results

❖ Algorithm Assessment

Reference datasets

a) BGC-Argo (global scale; >40000 radiometric profiles at 4 bands available since 2012, https://maps.biogeochemical-argo.com/bgcargo/)

b) ESA Ocean Colour Climate Change Initiative (ESA-OC-CCI; esa-oceancolour-cci.org)

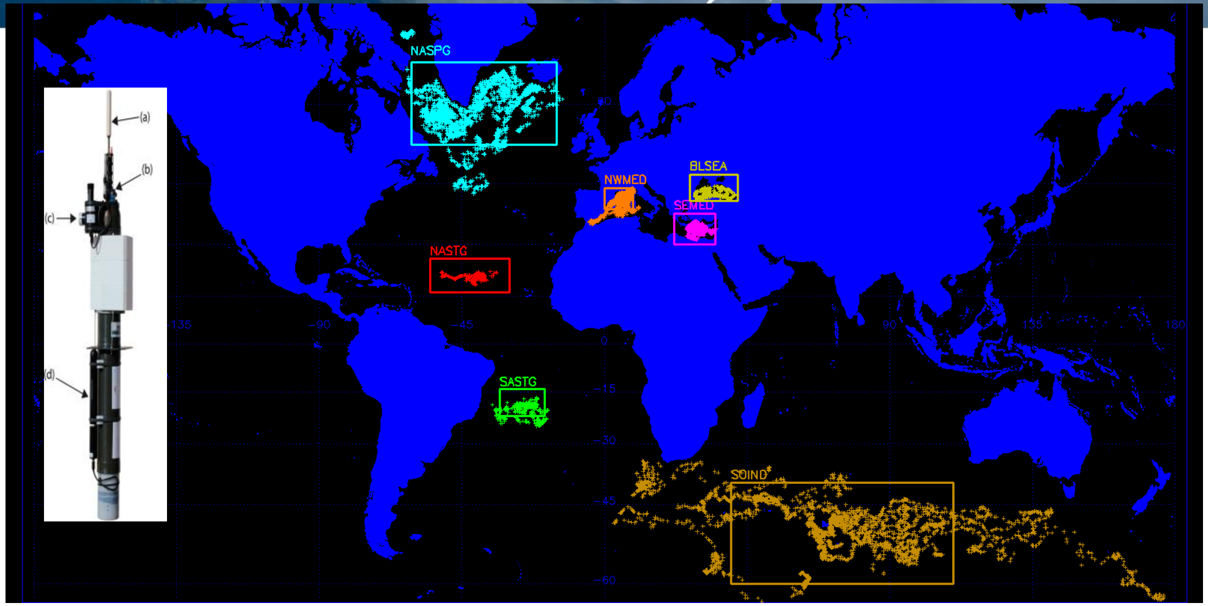

AEOLUS L1B Dataset, Baseline 11: April 2020 - March 2021.

Region\Season	DJF	MAM	JJA	SON	ALL
NASTG	193	146	127	252	**718**
SASTG	212	130	140	79	561
NWMED	8	4	44	17	73
SEMED	34	40	144	64	282
NASPG	0	0	3	1	4
BLSEA	1	4	22	10	37
SOIND	24	9	3	19	55

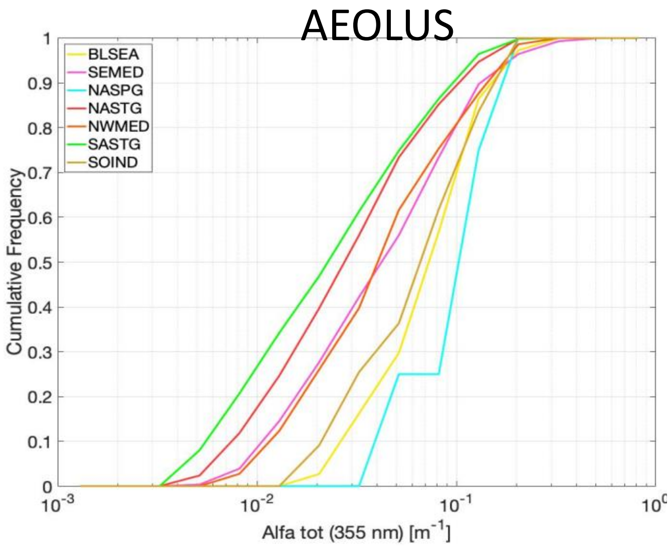

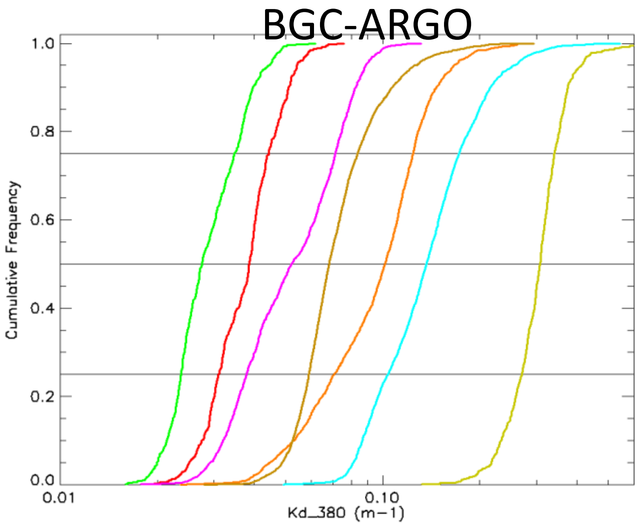

Results

❖ Match-up Assessment

- ESA-OC-CCI @ 412 nm scaled @ 355 nm
- Dataset: April 2020 - March 2021
- only AEOLUS data with $\Delta Bw/Bw \leq 1$

Match-up criteria

1) **Temporal matching**: ±24 hrs
2) **Spatial matching**: 5x5 pixels (20x20 km) around the AEOLUS measurement.
3) **Number of valid pixels**: ≥4 out of 25

AEOLUS

$$\Delta a(355) = a_{tot}(355) - a_{w}(355) - (0.052 \cdot Chl\text{-}a^{0.635})$$

$$\Delta a(355) = a_{CDOM}(355) + a_{NAP}(355)$$

$$a_{CDOM}(355) \gg a_{NAP}(355)$$

$$\boldsymbol{a_{CDOM}(355)} \approx \Delta a(355)$$

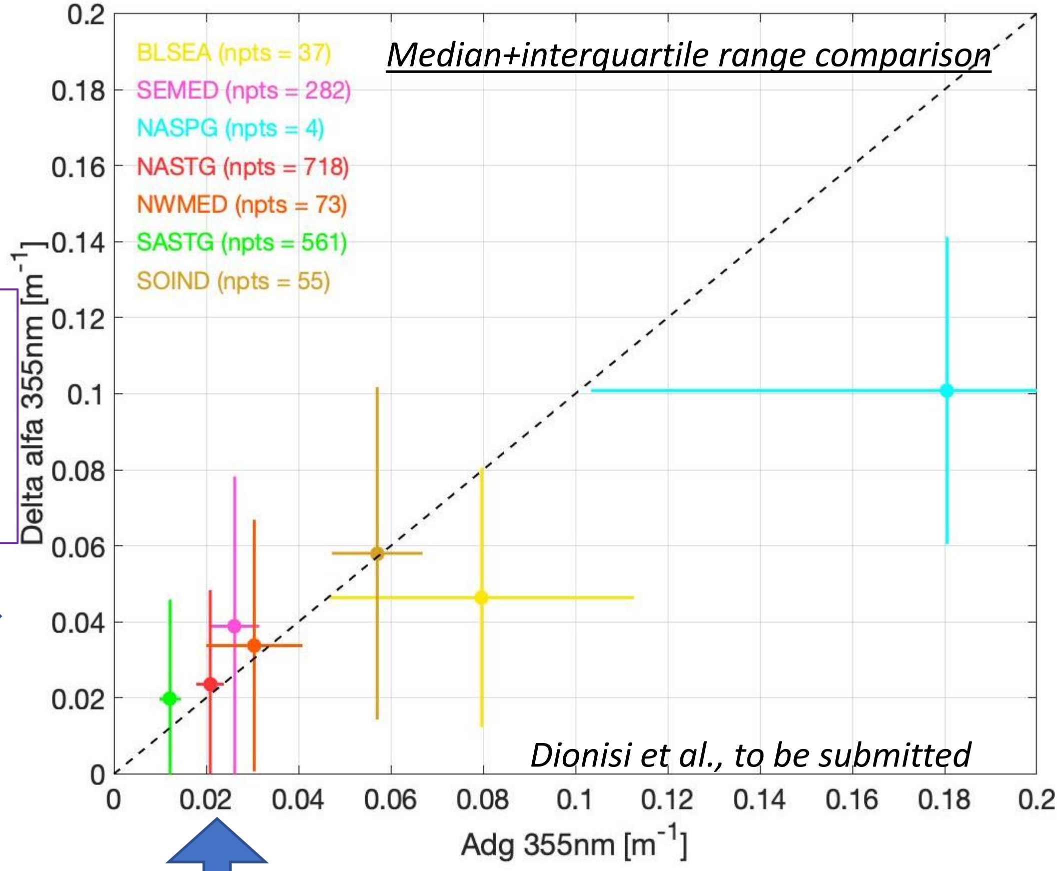

ESA-OC-CCI

$$a_{dg}(412) = a_{CDOM}(412) + a_{NAP}(412)$$

$$a_{CDOM}(412) \gg a_{NAP}(412)$$

$$\boldsymbol{a_{CDOM}(355)} \approx a_{dg}(412) \cdot \exp[-0.014(355 - 412)]$$

Conclusions

- ✓ Development of a status of the art modeling tool (LIOC)
- ✓ Demonstrated sensitivity of the AEOLUS measurements to marine optical properties
- ✓ AEOLUS OC prototype product in a spectral region (355 nm) not covered by operational OC products
- ✓ Overall demonstrated agreement between reference measurements and the proposed OC product

- ✗ Atmospheric disturbances (cloud and aerosol contamination) not properly accounted for
- ✗ Low SNR in the cloud free ground bin signal
- ✗ Limited spatial and temporal coverage
- ✗ HSRL not exploited (single channel (Mie) retrieval)
- ✗ In-water profiling capability not available

Roadmap

Applicability of the COLOR results to EarthCARE mission

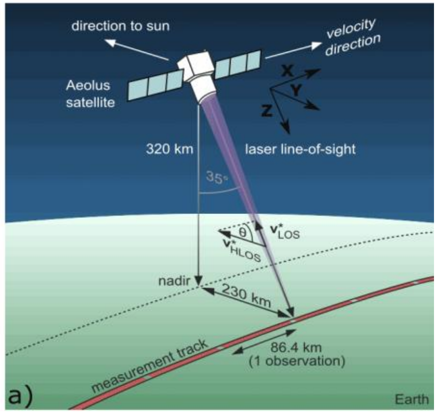

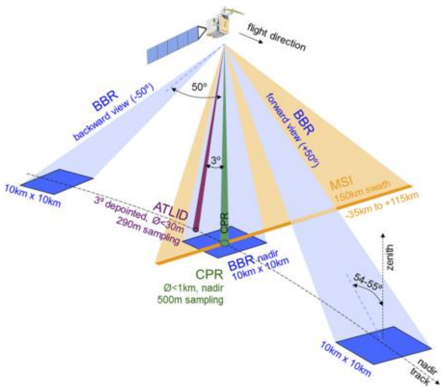

Main differences between AEOLUS and ATLID for OC application:

	ALADIN	**ATLID**	
❑ Vertical resolution:	500 m	**100 m**	Better separation of the atmospheric signal in the ground bin return (e.g. optimization of cloud and aerosols identification)
❑ Laser emitting angle:	35°	**3°**	Stronger surface return and signal propagation
❑ Acquisition channels:	-Co-polar Rayleigh A -Co-polar Rayleigh B -Co-polar Mie	-Co-polar Rayleigh -Co-polar Mie -**Total cross polar**	Optical characterization of the ocean particles through polarization capability
❑ Instruments on platform:	-	**-Cloud Profiling Radar** **-Multi-Spectral Imager** **-Broad-Band Radiometer**	Improvement of scene characterization (e.g. cloud detection)
❑ Local solar time (LST) sampling:	dawn/dusk	**day**/night	Large variability of the background signal. Marine diurnal cycle. OC information during nighttime. LST passage closer to OC satellite missions

Applicability of the COLOR results to EarthCARE mission

Actions to exploit COLOR's heritage for OC studies using EarthCARE

- Data analysis procedure
- LiOC radiative transfer tool
- Improved characterization of atmospheric (aerosols and clouds) disturbances
- Exploitation of High Spectral Resolution Lidar (HSRL) capabilities
- Exploitation of Polarization capabilities
- Possibility to implement Synergetic Inversion algorithm including, as input, active and passive measurements (OC missions).

Methods

❖ AEOLUS in-water algorithm

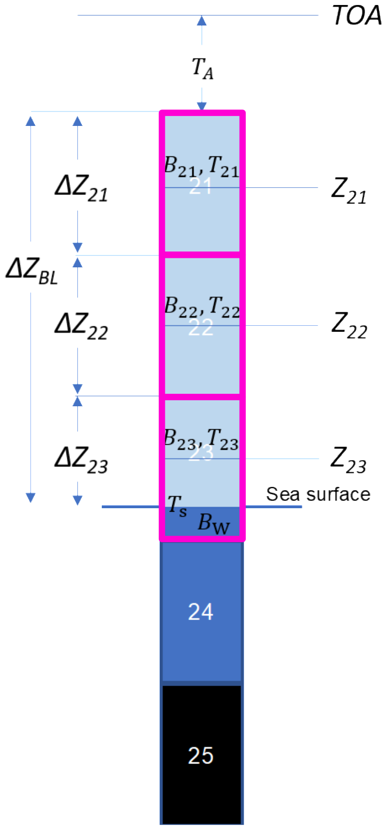

Elastic Backscatter Lidar AEOLUS-adapted inversion algorithm

Rationale: use the information in bins 21 and 22 to account for the instrumental and atmospheric contribution in the bin 23 signal

INPUTS: (**Mie channel**) Range Corrected Signals (S^*_{xx}) and geometry of bins 21, 22, 23 ($z_{xx}, \Delta z_{xx}$)
ANCILLARY: Atmospheric density profile, surface wind (T_S^2), *sea temperature and salinity*, aerosols scale height (z_s) .
OUTPUT: sea water contribution (backscattering+extinction) to ground bin signal (B_w)

$$B_{wat} \approx \frac{(S^*_{23} - S^*_{22})}{S^*_{21}} \frac{B_{21m} n^2}{T_S^2 T_{BLm}^2} \frac{1}{T_{BLa}^2} \approx \frac{(S^*_{23} - S^*_{22})}{S^*_{21}} \frac{B_{21m} n^2}{T_S^2 T_{BLm}^2} e^{+\left(\frac{2\rho_0\, \sigma_{ext}}{\cos\theta}\left(e^{\frac{-z_{21}}{z_S}} \Delta z_{21} + e^{\frac{-z_{22}}{z_S}} \Delta z_{22} + e^{\frac{-z_{23}}{z_S}} \Delta z_{23}\right)\right)}$$

ASSUMPTIONS:

- Contributions of **sea surface backscattering** and of **sea bottom reflection** are **negligible**
- Sea surface trasmittance Ts = 0.97, independent from the direction of propagation
- Refractive index of sea water n=1.356 independent from salinity and temperature
- **Difference** between atmospheric **backscattering contribution of bin 22 and 23 is negligible** compared to the contribution of **sea water in bin 23**
- Atmospheric backscattering dominated by molecular contribution both for the optical thickness and for the shape of the phase function
- **Homogeneity of the aerosol type** in the Marine Atmospheric Boundary Layer (MABL) and **known vertical distribution**

Estimation of associated uncertainty

Identified sources of uncertainties:

- *Data homogeneity*
- ***Radiometric noise***
- *Cloud contamination*
- *Assumptions in the analytical model*
- *Aerosols*
- *$B_w \rightarrow \alpha$ conversion*

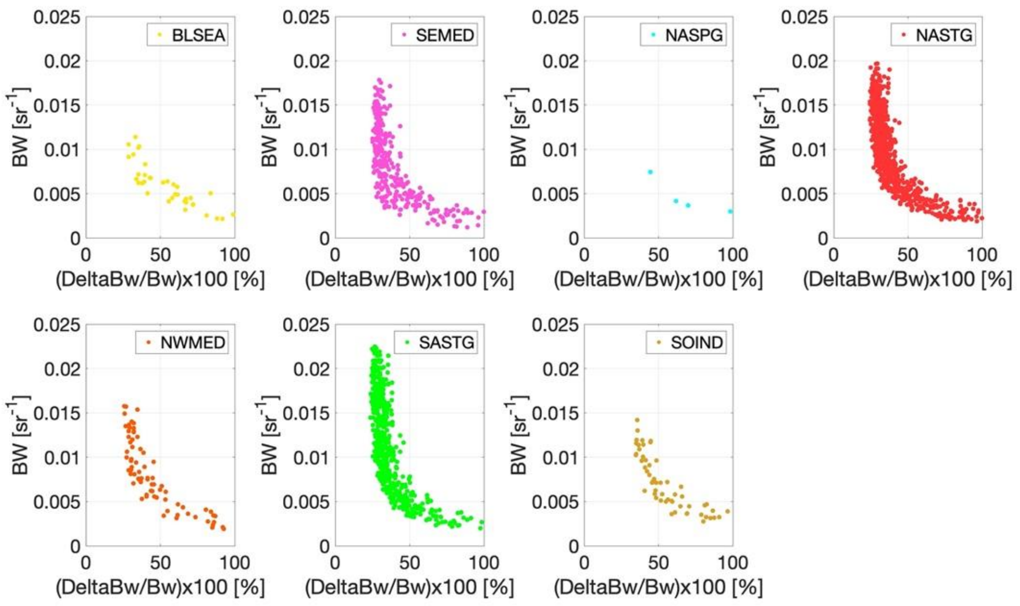

$$\Delta B_{wat}(355) = \sqrt{\left(\frac{\partial B_w}{dS^*_{21}}\right)^2 \cdot (\Delta S^*_{21})^2 + \left(\frac{\partial B_w}{dS^*_{22}}\right)^2 \cdot (\Delta S^*_{22})^2 + \left(\frac{\partial B_w}{dS^*_{23}}\right)^2 \cdot (\Delta S^*_{23})^2}$$

Associated uncertainty to the prototype product is based on the effect of radiometric noise recognized as major (and quantitatively documented) source of uncertainty.

A robust quantitative and detailed validation-based estimation of uncertainties of the AEOLUS OC product is not possible due to the small dimension of the comparison dataset.

Methods

❖ General approach: ground bin characterization

The potential information on ocean subsurface optical properties is contained in the AEOLUS ground bin volume (**Δr_{grd}**)

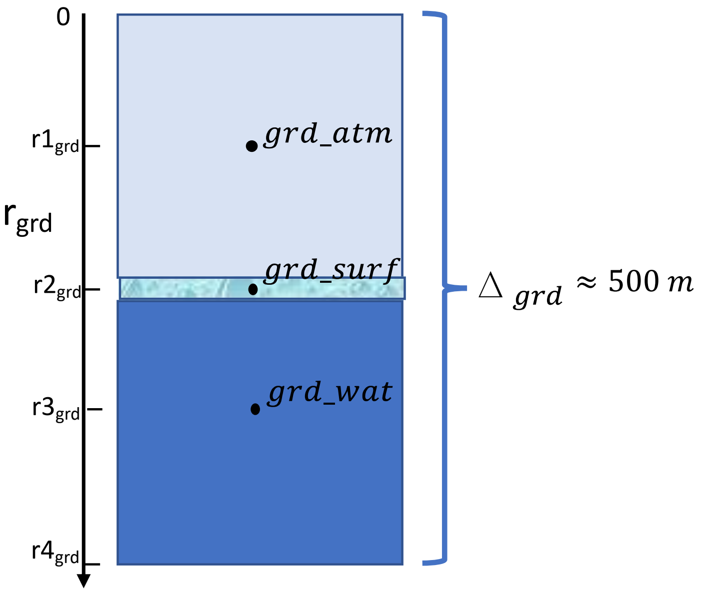

$$S_X(grd) = M_X \left[\frac{A}{\left(r_{atm} + \frac{\Delta r_{atm}}{n} \right)^2} \right] B_{grd} T_A^2(r_{atm}) + S_{bkd} \quad (1)$$

X= $Ray_{A,B}$

X= Mie

$$B_{grd} = B_{atm} + B_{srf} + B_{wat}(K_L, \beta_{wat}^{par}, \beta_{wat}^{mol}) \quad (2)$$

$$B_{wat} = \int_0^{r_{wat}} \beta_{wat}(\pi, r'_{wat})\, exp\left[-2 \int_0^{r'_{wat}} K_{LID}(r''_{wat}) dr''_{wat} \right] dr'_{wat} \quad (3)$$

This characterization is based on:

a) **Radiative transfer numerical modelling**

b) **AEOLUS data analysis**

Methods

❖ LiOC in-water forward model

Overview of the backward scheme for a_{tot} retrieval

1. LUT computed through forward MC simulations to determine $\mathbf{P_n}$ as a function of IOPs.

Chl-a	Δa log-uniformly varied between 0 and 15 m^{-1}												Ref. case	
	Pn	a1	Pn	a2	Pn	a3	Pn	a4	Pn	a5	Pn	a6	Pn	atot
0.001	1.92E-13	0.0012	8.48E-14	0.0212	2.49E-14	0.1012	5.39E-15	0.5012	1.09E-15	2.5012	1.82E-16	15.0012	1.83E-13	0.0025
0.003	1.75E-13	0.0014	8.19E-14	0.0214	2.49E-14	0.1014	5.43E-15	0.5014	1.10E-15	2.5014	1.83E-16	15.0014	1.54E-13	0.0041
0.01	1.46E-13	0.0021	7.73E-14	0.0221	2.49E-14	0.1021	5.49E-15	0.5021	1.11E-15	2.5021	1.86E-16	15.0021	1.18E-13	0.0078
0.03	1.20E-13	0.0037	6.98E-14	0.0237	2.48E-14	0.1037	5.62E-15	0.5037	1.14E-15	2.5037	1.91E-16	15.0037	8.62E-14	0.015
0.1	9.10E-14	0.0078	6.17E-14	0.0278	2.47E-14	0.1078	5.87E-15	0.5078	1.19E-15	2.5078	2.00E-16	15.0078	5.61E-14	0.0322
0.3	6.84E-14	0.0168	5.16E-14	0.0368	2.40E-14	0.1168	6.10E-15	0.5168	1.27E-15	2.5168	2.14E-16	15.0168	3.60E-14	0.0658
1	4.82E-14	0.0408	3.98E-14	0.0608	2.21E-14	0.1408	6.71E-15	0.5408	1.42E-15	2.5408	2.41E-16	15.0408	2.23E-14	0.146
3	3.49E-14	0.0934	2.96E-14	0.1134	2.04E-14	0.1934	7.11E-15	0.5934	1.68E-15	2.5934	2.87E-16	15.0934	1.33E-14	0.3047
10	2.33E-14	0.2334	2.12E-14	0.2534	1.61E-14	0.3334	7.70E-15	0.7334	2.19E-15	2.7334	3.90E-16	15.2334	8.19E-15	0.6873
30	1.51E-14	0.5405	1.42E-14	0.5605	1.23E-14	0.6405	7.65E-15	1.0405	2.69E-15	3.0405	4.88E-16	15.5405	5.08E-15	1.4524
100	7.62E-15	1.3586	7.18E-15	1.3786	6.65E-15	1.4586	5.27E-15	1.8586	2.33E-15	3.8586	5.40E-16	16.3586	2.91E-15	3.3173

2. The LUT entered through the observed **Chl–a** and $\mathbf{P_n}$ values

3. The a_{tot} value retrieved by interpolation

Chl-a ancillary

Aeolus

Chl–a	a_{tot}	P_n
c_1	a_1	p_1
…	..	…
c_N	a_N	p_N

Retrieved

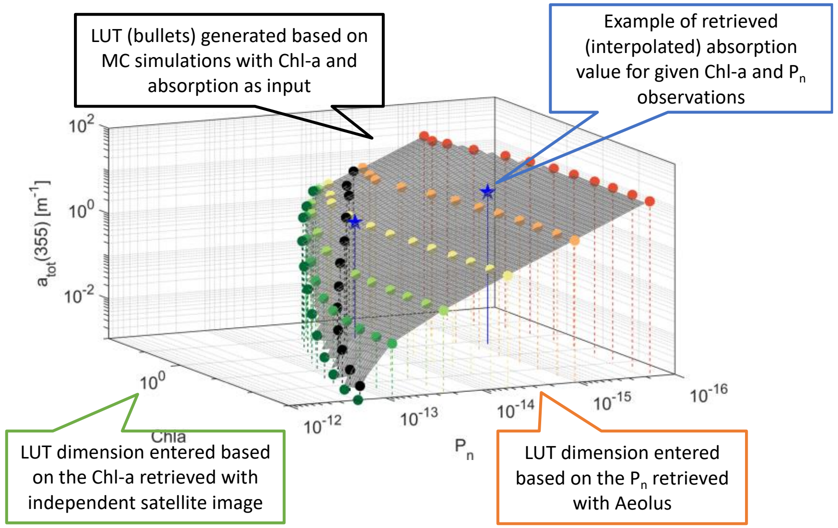

$$P_N = \mathbf{B}_{wat} \cdot \boldsymbol{\Delta\Omega}_r$$

Methods

❖ AEOLUS in-water algorithm

High Spectral Resolution Lidar approach

Objective: coupling the signals coming from Brillouin and Mie spectra (Rayleigh+Mie channels)

HSRL in water

$$S_{Mie} = M^{w}_{Mie}\left[\frac{A}{\left(r_{atm}+\frac{\Delta r_{atm}}{n}\right)^{2}}\right]\left(C^{w}_{4}\beta^{m}_{wat}+C^{w}_{3}\beta^{p}_{wat}\right)exp\left[-2\int_{0}^{r_{wat}}K_{LID}(r'_{wat})dr'_{wat}\right]T^{2}_{A}(r_{atm})$$

$$S_{Ray} = M^{w}_{Ray}\left[\frac{A}{\left(r_{atm}+\frac{\Delta r_{atm}}{n}\right)^{2}}\right]\left(C^{w}_{1}\beta^{m}_{wat}+C^{w}_{2}\beta^{p}_{wat}\right)exp\left[-2\int_{0}^{r_{wat}}K_{LID}(r'_{wat})dr'_{wat}\right]T^{2}_{A}(r_{atm})$$

$$\beta^{p}_{wat} = \beta^{m}_{wat}\left[\frac{S_{R}M^{w}_{Mie}C^{w}_{4}-M^{w}_{Ray}C^{w}_{1}}{M^{w}_{Ray}C^{w}_{2}-S_{R}M^{w}_{Mie}C^{w}_{3}}\right]$$

- ➢ Calibration and cross talk coefficients estimated for atmospheric application **cannot be used for the Brillouin scattering in water**
- ➢ **High variability** of the Rayleigh ground bin signal

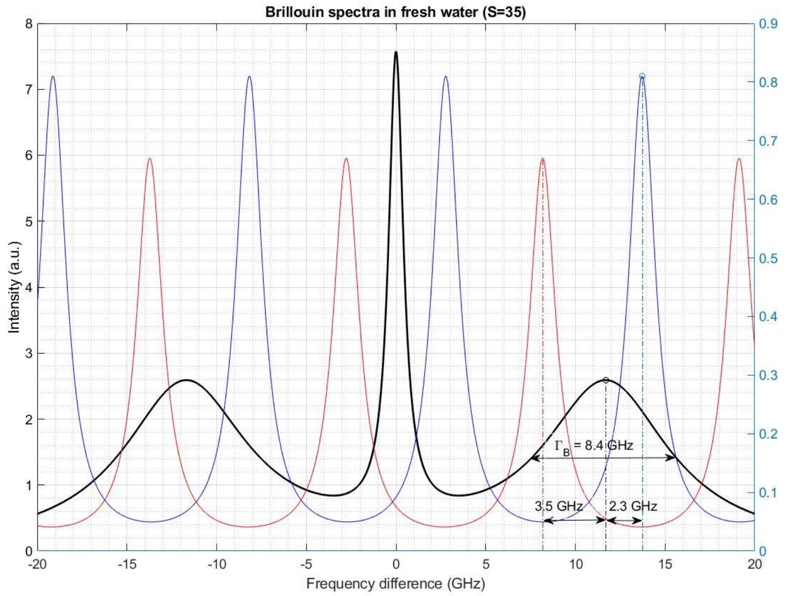

FWHM	1,78 GHz
FSR	10,95 GHz
Spacing between A and B	5,5 GHz
Filter A Peak Transmission	81 %
Filter B Peak Transmission	67 %